Comparing Different Ultrasound Imaging Methods for Breast Cancer Detection

Neslihan Ozmen, Robin Dapp, Michael Zapf, Hartmut Gemmeke, Nicole V. Ruiter, *Member, IEEE*, and Koen W. A. van Dongen

Abstract—Ultrasound is frequently used to evaluate suspicious masses in breasts. These evaluations could be improved by taking advantage of advanced imaging algorithms, which become feasible for low frequencies if accurate knowledge about the phase and amplitude of the wave field illuminating the volume of interest is available. In this study, we compare five imaging and inversion methods: time-of-flight tomography, synthetic aperture focusing technique, backpropagation, Born inversion, and contrast source inversion. All methods are tested on the same full-wave synthetic data representing a 2-D scan using a circular array enclosing a cancerous breast submerged in water. Of the tested methods, only contrast source inversion yielded an accurate reconstruction of the speed-of-sound profile of the tumor and its surroundings, because only this method takes effects such as multiple scattering, refraction, and diffraction into account.

I. Introduction

ULTRASOUND breast imaging was shown to be successful in detecting tumors in dense breasts which may be missed using mammography [1], [2]. The application of ultrasound as a noninvasive imaging modality for breast cancer detection was already investigated in the seventies and eighties, and led to the development of ray-based CT [3]–[6] and Doppler imaging methods [7] for breast cancer detection. In addition, hybrid methods and systems were developed which obtain pulse echo, attenuation, and speed-of-sound images simultaneously [8]. Taking advantage of these early successes, fully-automated ultrasound breast scanning systems were developed [9]–[13]. Typically, these systems allow for reproducible measurements when accurate knowledge about the scanning system and the field illuminating the volume of interest (phase and amplitude in absence of any contrast) is available. Having access to this information is an important condition for applying advanced 3-D imaging algorithms. Although the early imaging methods are typically computationally efficient, they do not take into account many of the phenomena associated with the wave nature of the ultrasound field, e.g., diffraction, refraction, and multiple scattering. To overcome these limitations, various methods have been developed which do take into account (with varying degree) the (full-)wave nature of the field [14]–[19].

This study aims to compare five different imaging methods—with varying complexity and underlying assumptions—for localizing and characterizing the tumor in a breast. Time-of-flight tomography (TOFT) is the only ray-based method investigated [20], [21]. With imaging, recorded travel times are related to a known matrix (containing information about the locations of all sources and receivers) and an unknown speed-of-sound map. This matrix-vector problem is successively solved using an iterative minimization algorithm [22], which uses total variation for regularization. The remaining four methods are wave-based. Synthetic aperture focusing technique (SAFT), also known in literature as migration or delay-and-sum imaging, is typically used to compute reflectivity images [23]. The second wave-based method tested is backpropagation (BP). This single-step frequency-domain method is based on the reverse process of the forward problem, i.e., computation of the pressure field given a known source distribution [14], [24], [25]. This method yields results similar to those obtained in the first iteration step of the Born inversion (BI) method. With this method, the inverse scattering problem is formulated in the frequency domain via an integral equation. This equation is a linearized version of the full-wave or nonlinear integral equation and is solved iteratively for the unknown contrast function [14], [26]. Finally, a full-wave nonlinear inversion method is tested. For this, the contrast source inversion (CSI) method is used. This iterative method operates beyond the Born approximation and solves the full nonlinear inverse problem [15], [27].

To investigate the potential of each method, they are all tested on two data sets; a noise-free synthetic data set and one with 1% white noise. Both data sets represent the same cross-sectional scan of a breast model built from a magnetic resonance imaging (MRI) scan of a cancerous breast [28]. Although all methods are applicable in 3-D, we have used a 2-D example for ease of comparison. To cope with noise, several techniques may be applied, varying from regularization techniques, such as total variation, up to spatial filtering techniques as a post-processing step. Testing these different regularization and filtering methods is a different topic and is considered to be beyond the scope of the presented work.

II. Theory

To ease the comparison between the various imaging methods, only lossless media showing a spatially varying speed of sound $c(\boldsymbol{x})$ are considered. For these media, the propagation and scattering of acoustic wave fields may be described in the time domain via the scalar wave equation

$$\nabla^2 p(\boldsymbol{x},t) - \frac{1}{c^2(\boldsymbol{x})}\frac{\partial^2 p(\boldsymbol{x},t)}{\partial t^2} = -S(\boldsymbol{x},t), \qquad (1)$$

where $p(\boldsymbol{x},t)$ is the acoustic pressure field at the location $\boldsymbol{x}$ and time t, and $S(\boldsymbol{x},t)$ describes the primary source generating the acoustic wave field. Typically, these sources are located on a surface $\mathbb{S}$ enclosing the spatial domain of interest $\mathbb{D}$, see Fig. 1. Transforming (1) to the frequency domain yields the Helmholtz equation for heterogeneous media,

$$\nabla^2 \hat{p}(\boldsymbol{x}) + \frac{\omega^2}{c^2(\boldsymbol{x})}\hat{p}(\boldsymbol{x}) = -\hat{S}(\boldsymbol{x}), \qquad (2)$$

where ω is the angular frequency and where the caret symbol $\hat{\ }$ is used to denote quantities defined in the frequency domain. The pressure field $\hat{p}(\boldsymbol{x})$ may be decomposed into an incident field $\hat{p}^{\mathrm{inc}}(\boldsymbol{x})$, which is the field generated by the primary source $\hat{S}(\boldsymbol{x})$ and propagating in a homogeneous background medium with speed of sound c_0, and a correction term referred to as the scattered field $\hat{p}^{\mathrm{sct}}(\boldsymbol{x})$ [29], [30]; hence,

$$\hat{p}(\boldsymbol{x}) = \hat{p}^{\mathrm{inc}}(\boldsymbol{x}) + \hat{p}^{\mathrm{sct}}(\boldsymbol{x}). \qquad (3)$$

By taking advantage of Gauss's theorem, it may be shown that the scattered field $\hat{p}^{\mathrm{sct}}(\boldsymbol{x})$ equals

$$\hat{p}^{\mathrm{sct}}(\boldsymbol{x}) = \omega^2 \int\limits_{\boldsymbol{x}' \in \mathbb{D}} \hat{G}(\boldsymbol{x}-\boldsymbol{x}')\hat{p}(\boldsymbol{x}')\chi(\boldsymbol{x}')\mathrm{d}\,V(\boldsymbol{x}'), \qquad (4)$$

where $\hat{G}(\boldsymbol{x}-\boldsymbol{x}')$ is the Green's function describing the impulse response of the background medium, and where the contrast function $\chi(\boldsymbol{x}')$ describes the variations in speed of sound due to the presence of objects in the spatial domain $\mathbb{D}$. This contrast function is defined as

$$\chi(\boldsymbol{x}') = \frac{1}{c^2(\boldsymbol{x}')} - \frac{1}{c_0^2}. \qquad (5)$$

Note that for the considered problem there is no need to use absorbing boundary conditions or perfectly matched layers [31] because the applied Green's function satisfies the Sommerfeld radiation condition.

Eqs. (3) and (4) represent a Fredholm integral equation of the second kind. The situation in which both the incident field $\hat{p}^{\mathrm{inc}}(\boldsymbol{x})$ and the contrast function $\chi(\boldsymbol{x}')$ are known, but where the pressure field $\hat{p}(\boldsymbol{x})$ is unknown, is referred to in the literature as the forward problem. This is a linear
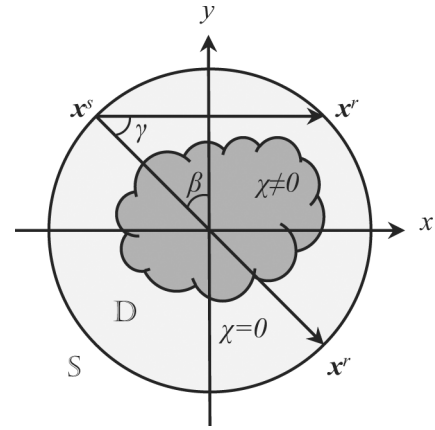

Fig. 1. Schematic representation of the scanning system. Sources and receivers are located at $\boldsymbol{x}^{\mathrm{s}}$ and $\boldsymbol{x}^{\mathrm{r}}$ on a surface $\mathbb{S}$ enclosing the domain $\mathbb{D}$. The latter domain is the region of interest where the contrast function χ may be nonzero.

inverse problem, which may be solved using a conjugate gradient solution method [32]. However, with imaging, the unknown contrast function $\chi(\boldsymbol{x}')$ is reconstructed from the pressure field $\hat{p}(\boldsymbol{x})$ measured by the receivers located in the spatial domain $\mathbb{S}$. Because both the contrast function and the pressure field inside the integral are unknown, imaging represents a nonlinear inverse problem. Next, five imaging methods will be tested by reconstructing the interior of the breast by solving the nonlinear inverse problem approximately or fully.

III. Methods

A schematic representation of the scanning system is shown in Fig. 1. Sources and receivers are located in the domain $\mathbb{S}$ at $\boldsymbol{x}^{\mathrm{s}}$ and $\boldsymbol{x}^{\mathrm{r}}$, respectively. The domain $\mathbb{S}$, referred to as the data domain, encloses the region of interest $\mathbb{D}$, referred to as the object domain, containing the objects.

A. Time-of-Flight Tomography (TOFT)

If the approximation is made that the pressure field travels along straight paths or rays, spatial variations in the speed of sound will lead to a phase shift of the measured signal, i.e., a change in travel time, as compared with a wave traveling in a homogeneous background medium. Within this approximation, the forward problem may be formulated as a Radon transform in a single (x,y)-plane:

$$\begin{aligned} P_\beta(\gamma) = \int\limits_{(x,y)\in\mathbb{D}} \frac{1}{c(x,y)}\delta[x\cos(\beta+\gamma) \\ + y\sin(\beta+\gamma) - R\sin(\gamma)]\mathrm{d}x\mathrm{d}y, \end{aligned} \qquad (6)$$

where $P_\beta(\gamma)$ is the travel time for a wave propagating from the source to the receiver, $\delta(\cdot)$ is Dirac's delta function, R is the radius of the circle on which the transducers are positioned, β is the angle between the y-axis and the

transmitter, and γ is the position of a ray in a fan beam. During imaging, a speed-of-sound profile of the region of interest may be obtained from the measured projections $P_\beta(\gamma)$ using the inverse of this Radon transform [6], [14].

A solution for the speed-of-sound profile may also be obtained by first casting the problem as a vector-matrix problem, where the time-of-flight measurements denoted by the vector $\mathbf{b}$ are connected via the matrix $\mathbf{A}$ to the slowness profile $\mathbf{s}$, which is the reciprocal of the speed of sound $\mathbf{c}$. The resulting equation is

$$\mathbf{As} = \mathbf{b}. \tag{7}$$

Next, an image of the speed-of-sound profile may be computed using an iterative scheme that minimizes the misfit between the actual or measured time-of-flight measurements $\mathbf{b}$ and the computed time-of-flight measurements based on the reconstructed slowness vector $\mathbf{s}$ [20]. This misfit may be expressed using the error $\mathbf{E}$:

$$\mathbf{E} = \|\mathbf{As} - \mathbf{b}\|^2, \tag{8}$$

where $\|\cdot\|$ is the L_2-norm. The advantage of an iterative approach is that it allows one to constrain possible solutions or to emphasize certain features of the reconstruction. To regularize our inverse problem, it is assumed that the reconstructed speed-of-sound profile is smooth. This constraint is included in the error $\mathbf{E}$ by considering the gradient or total variation (TV) of the reconstructed speed-of-sound vector, denoted as $\|\mathbf{c}\|_{\mathrm{TV}}$ [22]. Taking TV as an additive constraint, the error $\mathbf{E}$ given in (8) changes into

$$\mathbf{E} = \|\mathbf{As} - \mathbf{b}\|^2 + \lambda\|\mathbf{c}\|_{\mathrm{TV}}^2, \tag{9}$$

with weighting parameter λ [21]. To minimize this error functional, the TVAL3 algorithm [22], which employs an augmented Lagrangian method for optimization, is used. The iterative scheme is aborted as soon as the variation in the error $\mathbf{E}$ between two consecutive iterations drops below a predefined threshold ε.

B. Synthetic Aperture Focusing Technique (SAFT)

In situations in which only reflectivity images showing the boundary of an object are needed, the synthetic aperture focusing technique (SAFT), or delay-and-sum imaging, is adequate. With this method, the location of the object is determined in a straightforward manner by considering the time required for a wave to travel from the source at $\boldsymbol{x}^{\mathrm{s}}$ via the boundary of an object to the receiver at $\boldsymbol{x}^{\mathrm{r}}$. Combining several source/receiver combinations leads to constructive and destructive interference of the displayed reflected field, revealing the boundary of the object. Hence, the vector χ^{SAFT} representing the contrast function is obtained via

$$\chi^{\mathrm{SAFT}} = \sum_{j,\mathbf{t}} \mathbf{p}_j^{\mathrm{sct}}(\mathbf{t})\delta(c_0\mathbf{t} - |\boldsymbol{x}^{\mathrm{s}} - \boldsymbol{x}| - |\boldsymbol{x}^{\mathrm{r}} - \boldsymbol{x}|), \tag{10}$$

where a summation over all source/receiver combinations j and discrete time samples $\mathbf{t}$ of the measured field $\mathbf{p}_j^{\mathrm{sct}}(\mathbf{t})$ is made, and where $|\cdot|$ is the Euclidean length of a vector.

There are two important conditions for retrieving useful images with this method. First, the amount of multiple scattering should be limited; the presence of multiple scattering in the measured data will give rise to ghost objects in the image. Second, the maximum phase shift caused by variations in the speed of sound between the object and the embedding should be smaller than π; larger variations will destroy the constructive/destructive interference principle and may give rise to an aberrant positioning of the object. The latter aspect may be weakened by replacing the speed of sound of the embedding c_0 with an effective speed of sound; e.g., based on the average travel times measured with transducers in the presence of the object.

C. Backpropagation (BP)

Integral equation (3) and (4) can be linearized by replacing the unknown field $\hat{p}(\boldsymbol{x})$ within the integrand by the known incident field $\hat{p}^{\mathrm{inc}}(\boldsymbol{x})$. Application of this approximation has the effect that both multiple scattering and phase shifts caused by the spatially varying speed of sound are neglected. In the literature, this approximation is referred to as the Born approximation, and the resulting integral equation simplifies to

$$\hat{p}^{\mathrm{sct}}(\boldsymbol{x}) = \omega^2 \int_{\boldsymbol{x}'\in\mathbb{D}} \hat{G}(\boldsymbol{x} - \boldsymbol{x}')\hat{p}^{\mathrm{inc}}(\boldsymbol{x}')\chi(\boldsymbol{x}')\mathrm{d}A(\boldsymbol{x}'). \tag{11}$$

Recasting (11) into operator form yields the expression

$$\hat{\mathbf{p}}_j^{\mathrm{sct}} = \mathbf{M}[\chi], \tag{12}$$

where $\mathbf{M}$ represents the integral operator. To reconstruct χ from a set of measurements of $\hat{\mathbf{p}}_j^{\mathrm{sct}}$, we minimize the error $\mathbf{E}$ expressed as

$$\mathbf{E} = \left\|\hat{\mathbf{p}}_j^{\mathrm{sct}} - \mathbf{M}[\chi]\right\|_{\mathbb{S}}^2 \tag{13}$$

$$= \left\|\hat{\mathbf{p}}_j^{\mathrm{sct}}\right\|_{\mathbb{S}}^2 + \|\mathbf{M}[\chi]\|_{\mathbb{S}}^2 - 2\Re\langle\hat{\mathbf{p}}_j^{\mathrm{sct}}, \mathbf{M}[\chi]\rangle_{\mathbb{S}}, \tag{14}$$

where $\langle\cdot,\cdot\rangle_{\mathbb{S}}$ and $\|\cdot\|_{\mathbb{S}}$ are the inner product and L_2-norm on the data domain $\mathbb{S}$, respectively. To minimize the error $\mathbf{E}$, the last term on the right-hand side of (14), viz. $2\Re\langle\mathbf{p}_j^{\mathrm{sct}}, \mathbf{M}[\chi]\rangle_{\mathbb{S}}$, should be as large as possible. This is achieved by approximating the contrast function χ^{BP} by

$$\chi^{\mathrm{BP}} = \mathbf{M}^\dagger[\hat{\mathbf{p}}_j^{\mathrm{sct}}], \tag{15}$$

where the adjoint of operator $\mathbf{M}$, denoted by $\mathbf{M}^\dagger$, is

$$\mathbf{M}^{\dagger}[\hat{\mathbf{p}}_j^{\mathrm{sct}}] = \sum_{j,\omega} \omega^2 [\hat{\mathbf{p}}_j^{\mathrm{inc}}(\boldsymbol{x}')\hat{G}(\boldsymbol{x}^{\mathrm{r}} - \boldsymbol{x}')]^* \hat{\mathbf{p}}_j^{\mathrm{sct}}(\boldsymbol{x}^{\mathrm{r}}), \quad (16)$$

with the symbol * representing the complex conjugate. Note that backpropagation is very similar to the frequency-domain formulation of SAFT, which, formulated in the frequency domain, is

$$\chi^{\mathrm{SAFT}} = 8\pi \mathbf{M}^{\dagger}[\hat{\mathbf{p}}_j^{\mathrm{sct}}|\boldsymbol{x}^{\mathrm{s}} - \boldsymbol{x}'\|\boldsymbol{x}^{\mathrm{r}} - \boldsymbol{x}'\|], \quad (17)$$

in case the incident field $\hat{\mathbf{p}}_j^{\mathrm{inc}}(\boldsymbol{x}')$ is generated by a point source and equals $\hat{\mathbf{p}}_j^{\mathrm{inc}}(\boldsymbol{x}') = \hat{G}(\boldsymbol{x}^{\mathrm{s}} - \boldsymbol{x}')$.

D. Born Inversion (BI)

With Born inversion, the linearized integral equation (11) is solved iteratively for the unknown contrast function. Here, a conjugate gradient (CG) scheme [33] is applied to minimize the error functional presented in (13). Note that the first iteration step of the BI method is similar to the BP method.

E. Contrast Source Inversion (CSI)

The contrast source inversion method solves the nonlinear integral equation (3) and (4) without any approximations. The method assumes that the two unknowns, the contrast function and the total field inside the integrand, act together as a single contrast source that generates the scattering field. Consequently, the scattered and actual fields satisfy the following domain integral equations

$$\hat{p}^{\mathrm{sct}}(\boldsymbol{x}) = \omega^2 \int_{\boldsymbol{x}' \in \mathbb{D}} \hat{G}(\boldsymbol{x} - \boldsymbol{x}')\hat{w}(\boldsymbol{x}')\mathrm{d}A(\boldsymbol{x}') \quad \boldsymbol{x} \in \mathbb{S}, \quad (18)$$

$$\hat{p}(\boldsymbol{x}) = \hat{p}^{\mathrm{inc}}(\boldsymbol{x}) + \omega^2 \int_{\boldsymbol{x}' \in \mathbb{D}} \hat{G}(\boldsymbol{x} - \boldsymbol{x}')\hat{w}(\boldsymbol{x}')\mathrm{d}A(\boldsymbol{x}') \quad \boldsymbol{x} \in \mathbb{D}, \quad (19)$$

where the contrast source term $\hat{w}(\boldsymbol{x}')$ is defined as

$$\hat{w}(\boldsymbol{x}') = \chi(\boldsymbol{x}')\hat{p}(\boldsymbol{x}'). \quad (20)$$

Rewriting (18) and (19) in operator form yields

$$\hat{\mathbf{p}}_j^{\mathrm{sct}} = \mathbf{L}^{\mathbb{S}}[\hat{\mathbf{w}}_j], \quad (21)$$

$$\hat{\mathbf{p}}_j = \hat{\mathbf{p}}_j^{\mathrm{inc}} + \mathbf{L}^{\mathbb{D}}[\hat{\mathbf{w}}_j], \quad (22)$$

where $\mathbf{L}^{\mathbb{S}}$ and $\mathbf{L}^{\mathbb{D}}$ represent the integral operators. Multiplying both sides of (22) by χ and taking advantage of (20) yields

$$\chi\hat{\mathbf{p}}_j^{\mathrm{inc}} = \hat{\mathbf{w}}_j - \chi\mathbf{L}^{\mathbb{D}}[\hat{\mathbf{w}}_j]. \quad (23)$$

Eqs. (21) and (23) can be solved together for the unknown contrast source term $\hat{\mathbf{w}}_j$. To this end, an iterative scheme is employed which minimizes the error functional $\mathbf{E}$

$$\mathbf{E} = \mathbf{E}^{\mathbb{S}} + \mathbf{E}^{\mathbb{D}}, \quad (24)$$

where

$$\mathbf{E}^{\mathbb{S}} = \eta_{\mathbb{S}} \left\| \hat{\mathbf{p}}_j^{\mathrm{sct}} - \mathbf{L}^{\mathbb{S}}[\hat{\mathbf{w}}_j] \right\|_{\mathbb{S}}^2, \quad (25)$$

$$\mathbf{E}^{\mathbb{D}} = \eta_{\mathbb{D}} \left\| \chi\hat{\mathbf{p}}_j^{\mathrm{inc}} - \hat{\mathbf{w}}_j + \chi\mathbf{L}^{\mathbb{D}}[\hat{\mathbf{w}}_j] \right\|_{\mathbb{D}}^2, \quad (26)$$

with normalization factors

$$\eta_{\mathbb{S}} = \left(\left\| \hat{\mathbf{p}}_j^{\mathrm{sct}} \right\|_{\mathbb{S}}^2 \right)^{-1}, \quad (27)$$

$$\eta_{\mathbb{D}} = \left(\left\| \chi\hat{\mathbf{p}}_j^{\mathrm{inc}} \right\|_{\mathbb{D}}^2 \right)^{-1}. \quad (28)$$

After each update of the contrast source $\hat{\mathbf{w}}_j$, the initially unknown actual field $\hat{\mathbf{p}}_j$ within the entire spatial domain is recomputed. Finally, the contrast function χ^{CSI} is reconstructed from the updated contrast source $\hat{\mathbf{w}}_j$ and the recomputed field $\hat{\mathbf{p}}_j$ using a direct minimization method; hence

$$\chi^{\mathrm{CSI}} = \frac{\Re\langle\hat{\mathbf{p}}_j, \hat{\mathbf{w}}_j\rangle_{\mathbb{D}}}{\left\|\hat{\mathbf{p}}_j\right\|_{\mathbb{D}}^2}. \quad (29)$$

For both BI and CSI, the speed-of-sound profile $\mathbf{c}$ of the breast can be reconstructed from the contrast function $\chi^{\mathrm{BI/CSI}}$ via

$$\mathbf{c} = \frac{1}{\sqrt{\chi^{\mathrm{BI/CSI}} + c_0^{-2}}}. \quad (30)$$

IV. Configuration

All five imaging methods were tested on the same synthetic measurement data. The data represents a full 2-D tomographic scan of a cancerous breast using a circular array with a diameter of 258 mm containing 157 transducers; see Fig. 2. The 2-D speed-of-sound profile is based on a breast model retrieved from an MRI scan of a cancerous breast [28]. The applied speed-of-sound values of the different tissues [34] are given in Table I. The selected values for the different tissues are only indicative, because these values are typically difficult to measure. Fortunately, their absolute values are not important for this work, because it is about how accurately the different imaging methods can localize the various structures and reconstruct their original values.

The spatial domain contains 162×162 elements of size 1.7×1.7 mm. The A-scan length is 550.6 µs, which is discretized with a time step $\Delta t = 2.2$ µs. Each transducer acts as a point source, and generates a Gaussian modulated field with a center frequency $f_0 = 0.11$ MHz; hence, our spatial domain is discretized at 9 points per wavelength at the center frequency.
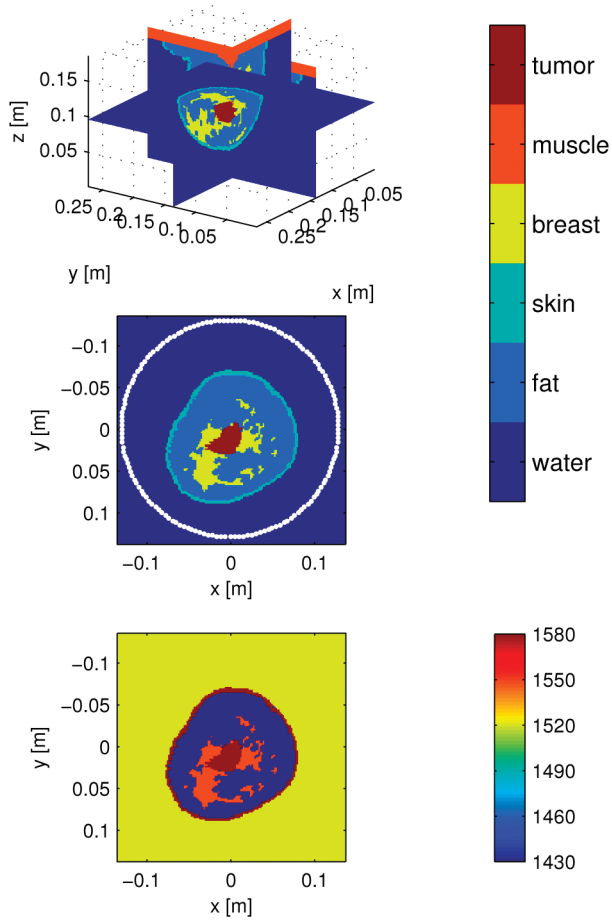
Fig. 2. Breast model built from a magnetic resonance imaging (MRI) scan of a cancerous breast [28]. The top and middle images display the different tissues. The middle image displays the planar domain of interest with the circular array (white dots); the bottom image displays the corresponding speed-of-sound profile [34].
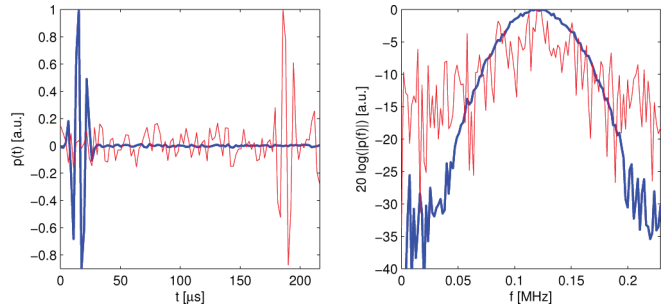

Fig. 3. Normalized A-scans (left) and their Fourier transforms (right). The blue curve is an A-scan with transmitter and receiver located at the same position; the red curve represents a through transmission measurement where the transmitter and receiver are separated by 180°.

Synthetic measurement data are computed in three ways. The first data set is obtained by solving the forward problem using a full-wave method. This method uses a CG scheme [32] to solve the frequency-domain integral equation (3) and (4) for each source position. Problems associated with the singularity of the Green's function are avoided by using its weak form [35]. Time-domain results are obtained by applying fast Fourier transforms. To emulate a real measurement, white noise has been added to the time-domain data. The white noise added has an amplitude equal to 1% of the maximum amplitude present in the entire data set. Examples of the synthetic measure-

ments are displayed in Fig. 3, where two normalized A-scans and their corresponding spectral content are shown.

The second data set only contains temporal phase shifts and is displayed in Fig. 4. This data set is computed using the Radon transform of (6) and is referred to as ray-based Radon data. Similar phase shifts are also computed from the full-wave data by cross-correlating the total field of the full-wave solution with the incident field. The cross-correlation is performed after interpolating the data by a factor of 128 by zero-padding the frequency-domain data. These phase shifts form the third data set, which is referred to as the full-wave Radon data. Both ray-based and full-wave Radon data are displayed in Fig. 4 and are only used to test TOFT. The two data sets look very similar. The observed differences are mainly due to diffraction, refraction, and interference, phenomena which are only modeled using the full-wave method.

V. RESULTS

All imaging methods are tested using the same full-wave synthetic data set. Their corresponding reconstructions are displayed in Fig. 5; the first two columns show normalized contrast functions in the absence and presence of 1% noise, whereas the last two columns show speed-of-

TABLE I. APPLIED SPEED OF SOUND VALUES
FOR DIFFERENT TISSUES [34].

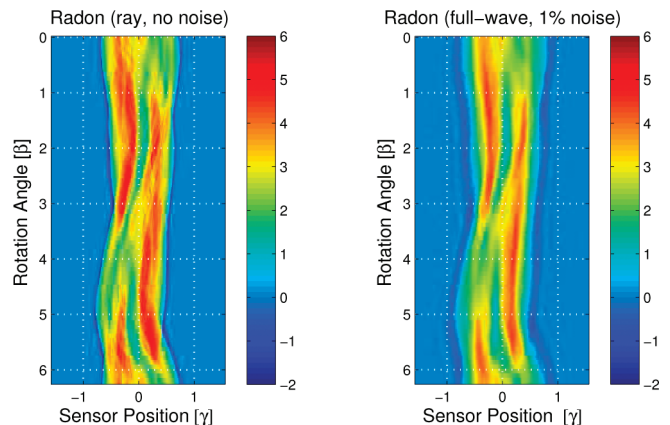| Tissue	Sound speed [m/s]
Tumor	1572
Breast	1540
Skin	1577
Fat	1437
Water	1520

Fig. 4. Phase shifts (in microseconds) representing the noise-free ray-based (left) and full-wave Radon data in the presence of 1% noise (right).
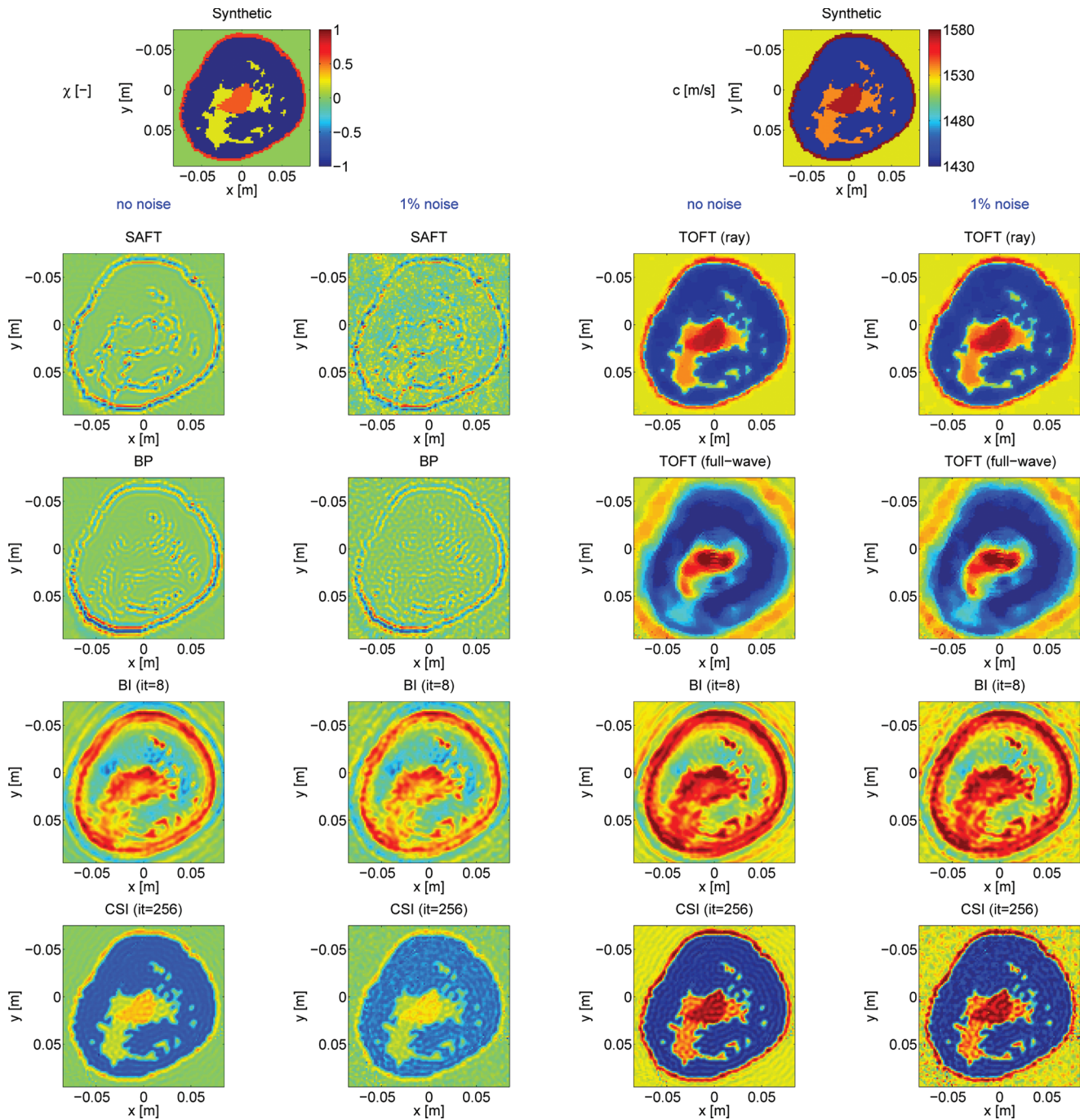
Fig. 5. Reconstructions obtained with all imaging methods using the full-wave solution in the absence and presence of 1% white noise. The first two columns show the contrast functions; the right two columns show speed-of-sound profiles in meters per second.

sound profiles. In addition to the full-wave data, TOFT has also been tested on the ray-based synthetic data set.

For SAFT and BP, all transducers are used as a source; however, only 39 receivers out of the 157 available transducers are used to obtain a B-scan. These receivers are always the direct neighbors of the transmitting one (including the zero-offset one). Although not thoroughly investigated by the authors, results presented by others [36] suggest that the angle over which these receivers are distributed should not exceed $\pi/2$. Because of the limited temporal resolution (low center frequency), both SAFT

and BP yield severely blurred images, mainly showing the water–breast interface. The negative effect of noise in the data is significant for SAFT and has only a limited effect on BP. Only SAFT reveals, up to a limited extent, the internal structure (amongst others, the tumor) of the breast.

Application of TOFT to the ray-based and the full-wave Radon data shows that the breast is clearly localized. However, only with the ray-based data the interior of the breast is imaged precisely, whereas application of the method on the full-wave data yields a blurred image. In all cases, the stopping criterion was set to $\varepsilon = 0.1 \cdot 10^{-3}$
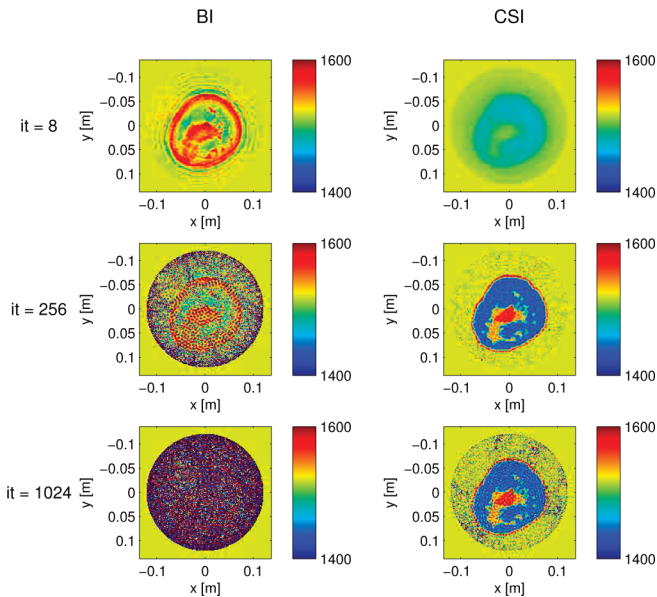
Fig. 6. Comparison of the results obtained with BI (left column) and CSI (right column) tested on the full-wave data set containing 1% white noise for increasing number of iterations (it): 8, 256, and 1024.

s^2. The results clearly confirm that for TOFT the effect of noise on the reconstruction is limited.

Finally, BI and CSI were tested on the full-wave data set. During imaging, all possible source/receiver combinations were used. To reduce the computational costs, only one frequency component, at the center frequency f_0 of the wave field, was used. The selected frequency corresponds to a wavelength equal to $\lambda = 13$ mm. With BI, the complete breast with the tumor is identified, unfortunately with wrong amplitudes. In addition, not all internal structures are reconstructed. With CSI, the breast, the tumor, and almost all internal structures are identified with (nearly) correct amplitudes. The effect of noise on the reconstruction by BI and CSI is also very limited.

Because both BI and CSI are iterative methods, the stopping criterion is a very important aspect. To show the stability of both methods, a comparison of BI and CSI for an increasing number of iterations (maximum number of iterations is set to 1024) is given in Fig. 6. BI diverges away from the correct solution after a small number of iterations, whereas CSI remains quite stable, despite the presence of noise.

To facilitate the comparison of the spatial resolution achieved with the different methods, a cross-sectional profile of the different results obtained is displayed in Fig. 7. These results clearly strengthen all previous observations. It shows that SAFT is capable of locating the contours of the breast and the tumor, whereas BP mainly finds the contours of the breast. TOFT yields an almost correct reconstruction on ray-based data, whereas it yields a severely blurred reconstruction on full-wave data. BI yields a correct localization of the breast and the tumor; however, the image is blurred and contains incorrect amplitudes. CSI is the only method that computes an almost perfect reconstruction for full-wave data. For a quantitative
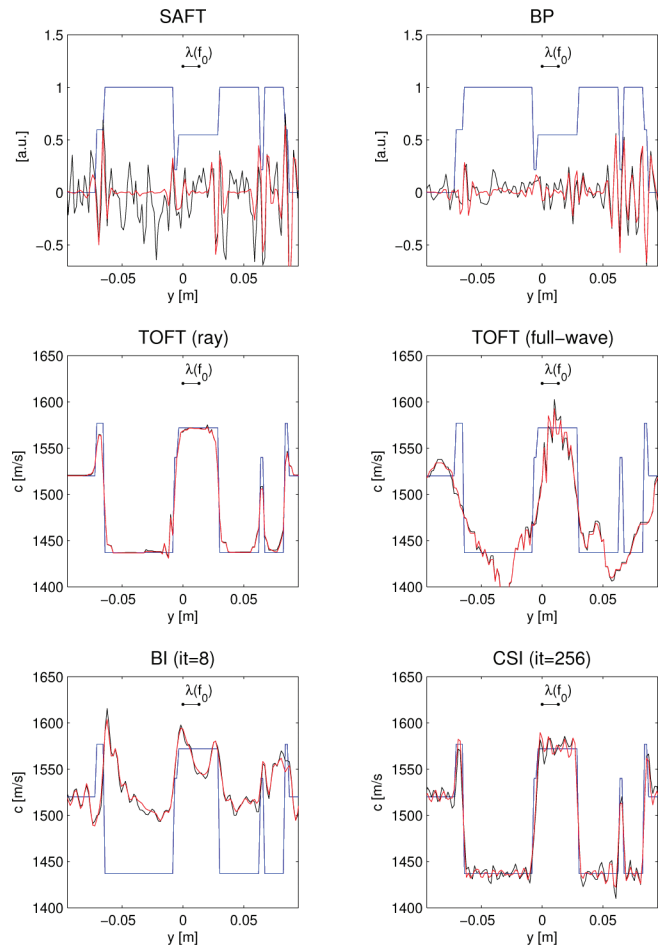

Fig. 7. Cross-sectional profiles along the line $x = 0$ m of the results presented in Fig. 5, displaying normalized contrast values for SAFT and BP, and speed-of-sound values for TOFT, BI, and CSI; the blue lines indicate the original profiles, the red and black lines indicate the reconstructed ones in the absence and presence of noise, respectively.

comparison, the root-mean-squared errors (RMSE) for TOFT, BI, and CSI are computed and displayed in Table II. These numbers confirm the previously mentioned observations and indicate that noise has hardly any effect on the obtained reconstructions. These results also indicate that the most accurate reconstruction for wave-based data is obtained by CSI, albeit at high computational expense.

VI. CONCLUSION

In this work, we compared five methods for breast ultrasound imaging: time-of-flight tomography (TOFT),

TABLE II. COMPARISON OF THE METHODS.

Method	RMSE [m/s] noise free	RMSE [m/s] 1% noise
TOFT (ray)	10	10
TOFT (full-wave)	25	25
BI	44	44
CSI	10	13

synthetic aperture focusing technique (SAFT), backprop-agation (BP), Born inversion (BI), and contrast source inversion (CSI). All methods are tested on the same synthetic data set, representing a 2-D tomographic scan of breast with a 4-cm-diameter tumor using a circular array with 157 transducers. The center frequency of the applied field is 0.11 MHz, which is considerably lower than is used in most ultrasound scanning systems. Finally, noise has been added to the synthetic data to avoid committing an inverse crime.

The obtained results show that SAFT is capable of locating the contours of the breast. Because of the low center frequency of the probing field, most of the remaining smaller structures are hardly visible. For an object with structures as small as 3 mm, as given by the ground truth of the tested object, the pulse should have a center frequency of approximately 500 kHz. Here, only 1/5 of that was applied. Consequently, the influence of the noise becomes significant in the reconstruction, despite the expected noise suppression of SAFT, which follows the square root of the number of applied A-scans. Because the method only displays the echogenicity of the interface of a contrast, quantitative information such as speed-of-sound values cannot be retrieved from the image. Because no correction is made for the applied waveform of the ultrasound field and the envelope of the reconstruction is not computed, the shape of the applied wave form is clearly visible in the image.

The observation made for SAFT is also valid for BP; it mainly succeeds in finding the contours of the breast. In general, multiple iteration steps are required to describe phenomena such as multiple scattering or phase shifts, and hence to reconstruct speed-of-sound profiles. Compared with SAFT, BP hardly displays any of the internal structures, which is due to the spherical decay present in the Green's function applied with BP. Omitting this spherical decay would yield similar images for both SAFT and BP.

TOFT is a ray-based method which allows for quantitative (speed of sound) imaging. The results show that the method is rather insensitive to noise in the data. Applying this method on ray-based data yield accurate reconstructions of both the location and amplitudes of the different objects. This may not be a surprise as both the forward and inverse problem are based on the same linear model. However, application of the method on the full-wave data yields severely blurred images with approximately correct amplitudes. This may be explained by comparing the computed Radon transforms using the ray model with the full-wave model; the full-wave Radon transform is smoother and does not show any of the detailed fine structures present in the ray-based Radon transform. This smoothing is caused by effects such as refraction, diffraction, scattering, and interference, which are present in the full-wave data and not modeled using the direct Radon transform. To test whether refraction plays a role, a modified TVAL3 inversion algorithm which includes refraction correction was applied [21]. Because the obtained results were identi-cal (data not shown), it may be concluded that refraction plays an insignificant role in this particular case, presumably because of the low center frequency.

The BI method yields a correct localization of the breast and can reconstruct most of the internal structures, albeit with wrong amplitudes. This is mainly because the presence of multiple scattering and the temporal phase shifts for waves traveling through the breast, as present in the full-wave data, are not included in the underlying computational model of the BI method; i.e., only the primary scattering is included and assumed to travel with the speed of sound of the embedding. An additional drawback of the BI method is the stopping criterion for the applied iterative scheme. As results show, the inversion is unstable and for real measurement data it will be unclear when to stop, especially because the error functional will remain decreasing during the inversion. However, by fitting the data in an incorrect model based on the Born approximation, the reconstruction will at some point start to diverge from the true solution. Application of regularization techniques such as total variation may reduce this effect and partly stabilize the inversion process.

Only with CSI accurate images were obtained; the breast including all its internal structures were reconstructed with nearly correct amplitudes. The images also show that objects with dimensions smaller than the wavelength of the probing field can be reconstructed. In addition, the effect of noise on the reconstruction was limited and may be further reduced using regularization techniques such as total variation [15].

Clearly, with all methods, smaller tumors and finer details will be detected by increasing the frequency of the probing field. The downside of increasing the center frequency is that it requires an increased number of receivers to avoid aliasing. For the given setup, the distance between two neighboring transducers is 0.4λ, yielding 157 transducers. Unfortunately, this number scales linearly with frequency.

The computational loads for SAFT, BP, and TOFT are of the same order of magnitude, and they are several orders of magnitude lower than the loads required for BI and CSI. At the same time, both BI and CSI only use a fraction of the available data; only one frequency component was used for the reconstruction.

In conclusion, effects such as scattering, diffraction, refraction, and phase shifts all play a role in breast ultrasound and should be taken into account during imaging. Of the five imaging methods tested on a full-wave data set, only CSI succeeds in computing accurate reconstructions because only CSI takes all of these effects into account.

References

[1] P. B. Gordon and S. L. Goldenberg, "Malignant breast masses detected only by ultrasound. a retrospective review," *Cancer*, vol. 76, no. 4, pp. 626–630, 1995.

[2] X. Ying, Y. Lin, X. Xia, B. Hu, Z. Zhu, and P. He, "A comparison of mammography and ultrasound in women with breast disease: A

receiver operating characteristic analysis," *Breast J.*, vol. 18, no. 2, pp. 130–138, 2012.

[3] G. H. Glover and J. C. Sharp, "Reconstruction of ultrasound propagation speed distributions in soft tissue: Time-of-flight tomography," *IEEE Trans. Sonics Ultrason.*, vol. 24, no. 4, pp. 229–234, Jul. 1977.

[4] G. H. Glover, "Computerized time-of-flight ultrasonic tomography for breast examination," *Ultrasound Med. Biol.*, vol. 3, no. 2–3, pp. 117–127, 1977.

[5] J. F. Greenleaf, "Computerized tomography with ultrasound," *Proc. IEEE*, vol. 71, no. 3, pp. 330–337, 1983.

[6] A. C. Kak and M. Slaney, *Principles of Computerized Tomographic Imaging*, vol. 33, Philadelphia, PA, USA: SIAM, 1988.

[7] J. F. Greenleaf, J. Ylitalo, and J. J. Gisvold, "Ultrasonic computed tomography for breast examination," *IEEE Eng. Med. Biol. Mag.*, vol. 6, no. 4, pp. 27–32, 1987.

[8] P. L. Carson, C. R. Meyer, A. L. Scherzinger, and T. V. Oughton, "Breast imaging in coronal planes with simultaneous pulse echo and transmission ultrasound," *Science*, vol. 214, no. 4525, pp. 1141–1143, 1981.

[9] K. J. Opielinski and T. Gudra, "Multi-parameter ultrasound transmission tomography of biological media," *Ultrasonics*, vol. 44, suppl., pp. e295–e302, 2006.

[10] H. Gemmeke and N. V. Ruiter, "3D ultrasound computer tomography for medical imaging," *Nucl. Instrum. Methods Phys. Res. A*, vol. 580, no. 2, pp. 1057–1065, 2007.

[11] N. Duric, P. Littrup, L. Poulo, A. Babkin, R. Pevzner, E. Holsapple, O. Rama, and C. Glide, "Detection of breast cancer with ultrasound tomography: First results with the computerized ultrasound risk evaluation (C.U.R.E.)," *Med. Phys.*, vol. 34, no. 2, pp. 773–785, 2007.

[12] M. André, J. Wiskin, D. Borup, S. Johnson, H. Ojeda-Fournier, and L. Olson, "Quantitative volumetric breast imaging with 3D inverse scatter computed tomography," in *Annu. Int. Conf. IEEE Engineering in Medicine and Biology Society (EMBC),* 2012, pp. 1110–1113.

[13] J. Rouyer, S. Mensah, E. Franceschini, P. Lasaygues, and J.-P. Lefebvre, "Conformal ultrasound imaging system for anatomical breast inspection," *IEEE Trans. Ultrason. Ferroelectr. Freq. Control*, vol. 59, no. 7, pp. 1457–1469, 2012.

[14] K. W. A. van Dongen and W. M. D. Wright, "A forward model and conjugate gradient inversion technique for low-frequency ultrasonic imaging," *J. Acoust. Soc. Am.*, vol. 120, no. 4, pp. 2086–2095, 2006.

[15] K. W. A. van Dongen and W. M. D. Wright, "A full vectorial contrast source inversion scheme for three-dimensional acoustic imaging of both compressibility and density profiles," *J. Acoust. Soc. Am.*, vol. 121, no. 3, pp. 1538–1549, 2007.

[16] F. Simonetti, L. Huang, N. Duric, and O. Rama, "Imaging beyond the Born approximation: An experimental investigation with an ultrasonic ring array," *Phys. Rev. E*, vol. 76, no. 3, art. no. 036601, 2007.

[17] P. Huthwaite and F. Simonetti, "High-resolution imaging without iteration: A fast and robust method for breast ultrasound tomography," *J. Acoust. Soc. Am.*, vol. 130, no. 3, pp. 1721–1734, 2011.

[18] J. Wiskin, D. T. Borup, S. A. Johnson, and M. Berggren, "Nonlinear inverse scattering: High resolution quantitative breast tissue tomography," *J. Acoust. Soc. Am.*, vol. 131, no. 5, pp. 3802–3813, 2012.

[19] M. C. Hesse, L. Salehi, and G. Schmitz, "Nonlinear simultaneous reconstruction of inhomogeneous compressibility and mass density distributions in unidirectional pulse-echo ultrasound imaging," *Phys. Med. Biol.*, vol. 58, no. 17, pp. 6163–6178, 2013.

[20] R. Dapp, M. Zapf, and N. V. Ruiter, "Geometry-independent speed of sound reconstruction for 3D USCT using apriori information," in *IEEE Int. Ultrasonics .*, 2011, pp. 1403–1406.

[21] R. Dapp, "Abbildungsmethoden für die Brust mit einem 3D-Ultraschall-Computertomographen," Ph.D. thesis, Faculty of Computer Science, Karlsruhe Institute of Technology, Karlsruhe, Germany, 2013.

[22] C. Li, W. Yin, and Y. Zhang. (Jul. 2013). TVAL3: TV minimization by Augmented Lagrangian and ALternating direction ALgorithms. [Online]. Available: http://www.caam.rice.edu/~optimization/L1/TVAL3/

[23] R. S. C. Cobbold, *Foundations of Biomedical Ultrasound*. New York, NY, USA: Oxford University Press 2007.

[24] H. Ammari, *An Introduction to Mathematics of Emerging Biomedical Imaging*, vol. 62. New York, NY, USA: Springer, 2008.

[25] A. J. Devaney, "A filtered backpropagation algorithm for diffraction tomography," *Ultrason. Imaging*, vol. 4, no. 4, pp. 336–350, 1982.

[26] A. Abubakar, P. M. van den Berg, and S. Y. Semenov, "A robust iterative method for born inversion," *IEEE Trans. Geosci. Rem. Sens.*, vol. 42, no. 2, pp. 342–354, 2004.

[27] P. M. van den Berg and A. Abubakar, "Contrast source inversion method: State of art," *Prog. Electromagn. Res.*, vol. 34, pp. 189–218, 2001.

[28] J. F. Bakker, M. M. Paulides, I. Obdeijn, G. C. van Rhoon, and K. W. A. van Dongen, "An ultrasound cylindrical phased-array for deep heating in the breast: Theoretical design using heterogeneous models," *Phys. Med. Biol.*, vol. 54, pp. 3201–3215, 2009.

[29] A. Gisolf and D. J. Verschuur, *The Principles of Quantitative Acoustical Imaging*. Houten, The Netherlands: EAGE Publications, 2010.

[30] J. T. Fokkema and P. M. van den Berg, *Seismic Applications of Acoustic Reciprocity*. Amsterdam, The Netherlands: Elsevier, 1993.

[31] E. J. Alles and K. W. A. van Dongen, "Perfectly matched layers for frequency-domain integral equation acoustic scattering problems," *IEEE Trans. Ultrason. Ferroelectr. Freq. Control*, vol. 58, no. 5, pp. 1077–1086, May 2011.

[32] N. Ozmen-Eryilmaz, L. Demi, E. J. Alles, M. D. Verweij, and K. W. A. van Dongen, "Modeling acoustic wave field propagation in 3D breast models," in *IEEE Int. Ultrasonics Symp.*, 2011, pp. 1700–1703.

[33] R. E. Kleinman and P. M. van den Berg, "Iterative methods for solving integral equations," *Radio Sci.*, vol. 26, no. 1, pp. 175–181, 1991.

[34] F. S. Foster, M. Strban, and G. Austin, "The ultrasound macroscope: Initial studies of breast tissue," *Ultrason. Imaging*, vol. 6, no. 3, pp. 243–261, 1984.

[35] P. Zwamborn and P. M. van den Berg, "The three-dimensional weak form of the conjugate gradient FFT method for solving scattering problems," *IEEE Trans. Microw. Theory Tech.*, vol. 40, no. 9, pp. 1757–1766, 1992.

[36] S. J. Norton and M. Linzer, "Ultrasonic reflectivity tomography: Reconstruction with circular transducer arrays," *Ultrason. Imaging*, vol. 1, no. 2, pp. 154–184, 1979.

Neslihan Ozmen received her B.S. degree in mathematics from Ankara University in 2005. After graduation, she followed a master's program in applied mathematics at the Middle East Technical University (METU), and in 2009 she received her M.S. degree in scientific computing. In June 2009, she moved to The Netherlands and joined the Laboratory of Acoustical Wavefield Imaging at Delft University of Technology for her Ph.D. studies, and received her Ph.D. degree in November 2014. Currently, she is employed as a postdoctoral researcher at Utrecht University. Her main research interests are nonlinear inverse problems, numerical modeling, and imaging.

Robin Dapp is a postdoctoral researcher at the Institute for Data Processing and Electronics (IPE), Karlsruhe Institute of Technology (KIT). He obtained a diploma and a Ph.D. degree in computer science from KIT. His research interests include ultrasound transmission tomography and finite-frequency tomography, image reconstruction, inverse problems, and numerical optimization.

Michael Zapf is a research associate at the Institute for Data Processing and Electronics (IPE), Karlsruhe Institute of Technology (KIT). He obtained a diploma in computer science from the University of Applied Science, Karlsruhe. His research interests include system development for ultrasound transmission tomography.
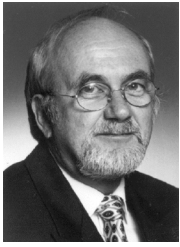
Hartmut Gemmeke was born in Northeim, Germany, on March 9, 1944. He studied exp. physics in Göttingen and Heidelberg and received his Ph.D. degree from the University of Heidelberg, Germany in 1971. Since 1990, he has been a supernumerary professor at the University of Heidelberg and since 1996 at the University of Karlsruhe. Since 2001, he has been the director of the Institute for Data Processing and Electronics at the Research Centre Karlsruhe. He has about 300 publications including 50 in medical techniques. After his retirement in 2010, he has been working as an advisor at the Karlsruhe Institute of Technology. He worked for the first ten years of his scientific career on nuclear physics (he invented a position-sensitive neutron detector), for the next ten years on neutrino physics (Karmen experiment), and then on astro-particle physics (Auger and AERA Experiment). His present research activities are focused on the investigation of 3-D ultrasound computed tomography for early breast cancer recognition.

Koen W. A. van Dongen received his M.Sc. degree from Utrecht University in 1997. From 1998 to 2002, he worked for T&A Survey on the development of a directional borehole radar system. This work resulted in a Ph.D. degree from Delft University of Technology in 2002. In 2002 and 2003, he worked as a postdoctoral researcher on ground-penetrating radar in the Laboratory of Electromagnetic Research at the same university. From 2003 to 2005, he worked as a Marie Curie Fellow on ultrasound thermometry in the Ultrasonic Research Group at University College Cork. In 2006, he moved to the Laboratory of Acoustical Wavefield Imaging, Delft University of Technology. His major research interests include imaging, inversion, and modeling of (nonlinear) acoustic wave fields for medical applications.

Nicole V. Ruiter received the Diploma degree in medical informatics from the University of Heidelberg and a Ph.D. degree in informatics from the University of Mannheim. She is a senior researcher at the Institute for Data Processing and Electronics at the Karlsruhe Institute of Technology. Her research interests include 3-D ultrasound imaging, medical image reconstruction, and biomechanical modeling. She has authored more than 100 papers in international journals and conferences. She is a member of IEEE and DEGA.